American Mineralogist, Volume 76, pages 1920–1930, 1991

Compositional constraints on the incorporation of Cl into amphiboles

Jean Morrison
Department of Geological Sciences, University of Southern California, Los Angeles, California 90089-0740, U.S.A.

Abstract

Compositional variations among 26 amphiboles in granulite-facies orthogneisses from the Adirondack Mountains of New York include a number of systematic cation-halogen correlations that provide information about compositional constraints on the incorporation of halogens, particularly Cl, into amphiboles. Two distinct groups of amphibole have been delineated on the basis of Cl content: Cl-rich amphiboles, which contain between 3.00 and 1.84 wt% Cl, and Cl-poor amphiboles, which contain between 0.47 and 0.05 wt% Cl. F contents range between 1.00 and 0.14 wt%.

The Cl-poor amphiboles clearly document Mg-Cl avoidance, yet among the Cl-rich amphiboles Mg-Cl avoidance is only weakly developed. Fe-F avoidance is not strongly developed among either the Cl-rich or Cl-poor amphiboles. Silica contents [expressed as Si/(Si + $^{[4]}$Al)] of Cl-rich amphiboles are distinctly lower than those of Cl-poor amphiboles: X_{Si} ranges from 0.793 to 0.770 in the Cl-poor group and from 0.761 to 0.742 in the Cl-rich group. Among the Cl-rich amphiboles, a strong inverse linear relation exists between X_{Si} and Cl.

The A site in all Cl-rich amphiboles is virtually full, with vacancies ranging from only 0.161 to 0.069. In general, the A site is occupied largely by K, and positive correlations between K and Cl exist among both Cl-rich and Cl-poor amphiboles.

If all Cl-rich and Cl-poor amphiboles equilibrated at the same temperature and if each group equilibrated with a fluid of relatively constant f_{HF}/f_{HCl}, then the compositional variations are interpreted to indicate that the effects of cation composition (e.g., X_{Mg}, X_{Si}) on the incorporation of Cl vary with significant differences in fluid composition. The data suggest that in relatively Cl-poor environments X_{Mg} is the predominant control on the incorporation of Cl; both X_{Si} and A site occupancy are important but less significant than X_{Mg}. Alternatively, in Cl-rich environments, X_{Si} and A site occupancy (particularly X_K) are more significant in determining Cl content than X_{Mg}.

Introduction

Cl and F have been shown to be important volatile components in a wide range of geologic processes including ore genesis, metamorphism, and magmatism. If the partitioning of Cl and F between a mineral and a fluid (or melt) can be quantitatively determined, then the mineral composition can be utilized to calculate the fugacity of halogen acid species (e.g., HCl and HF) that characterized the fluid during equilibration.

To date, experimental studies on the incorporation of halogens into minerals have focused primarily on biotite (Munoz and Ludington, 1974, 1977; Munoz and Swenson, 1981; Munoz, 1984; Volfinger et al., 1985) and apatite (Stormer and Carmichael, 1971; Korzhinskiy, 1981). Results from these experiments have been used to determine fluid compositions in a broad range of geologic processes (Munoz and Swenson, 1981; Yardley, 1985; Boudreau et al., 1986; Vanko, 1986; Sisson, 1987; Mora and Valley, 1989).

Results from experiments on biotite indicate that, unlike in apatite, variations in cation composition in addition to temperature and fluid composition play an extremely important role in Cl = F = OH exchange. Munoz (1984) summarized results from previous experimental work and data on natural biotite to derive expressions that relate variations in biotite cation composition to temperature and fluid composition (expressed as f_{HF}/f_{HCl}). These expressions indicate that the principal controls on halogen incorporation, in addition to temperature and fluid composition, are (1) the mole fraction Mg (X_{Mg} = Mg/total octahedral cations), (2) the mole fraction of siderophyllite where $X_{Sid} = [(^{[6]}X_{Al}/0.1670)\ (1 - X_{Mg})]$ (J. Munoz, personal communication), and (3) the mole fraction of annite $[X_{An} = 1 - (X_{Mg} + X_{Sid})]$.

These factors are thought to control the incorporation of halogens into the OH site as the result of the bonding between Cl and F and the octahedrally coordinated cations. Increased amounts of F are often correlated with increasing X_{Mg} or decreasing X_{Fe}, illustrating the Fe-F avoidance principle (Ramberg, 1952), and increasing Cl is often correlated with decreasing X_{Mg} or increasing X_{Fe}, reflecting the Mg-Cl avoidance principle. These avoid-

0003–004X/91/1112–1920$02.00

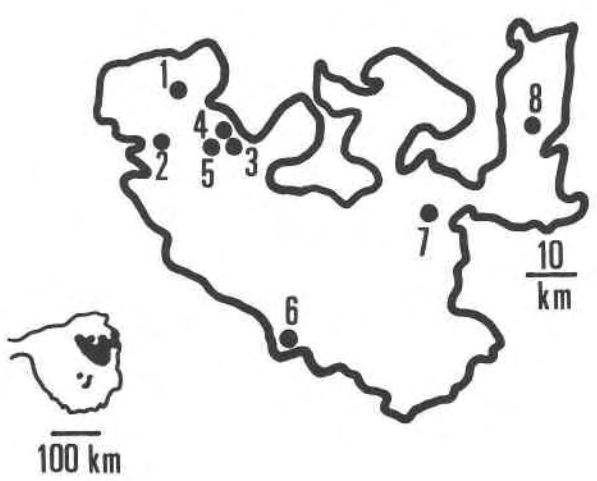

Fig. 1. Simplified map of the Marcy anorthosite massif in the Adirondack Mountains of northern New York showing sample locations for amphibole-bearing samples. Inset shows the location of the anorthosite massif (solid) in the Adirondack Mountains. Sample numbers on Figure 1 correspond to following samples: 1, 83-SR-4; 2, 83-SR-1; 3, 84-SR-10I; 4, 84-SR-8; 5, SL-11Y; 6, 84-SN-7; 7, 83-RB-11; 8, 83-AUS-20.

ances are interpreted to result from the preference of Fe for Fe-OH bonds rather than Fe-F bonds and from the preference of Mg for Mg-OH bonds rather than Mg-Cl bonds.

Volfinger et al. (1985) conducted experiments on the partitioning of Cl into biotite and concluded alternatively that the dimension of the OH site exerts fundamental control on the incorporation of Cl. Cl has a large ionic radius relative to F and OH, and Volfinger et al. (1985) argue that for the Cl ion to fit in the OH site, distortion of the pseudohexagonal tetrahedral ring that surrounds the Cl ion is necessary. This distortion is presumably enhanced by increased amounts of large octahedrally coordinated cations (e.g., Fe^{2+}) or small tetrahedrally coordinated cations [high $Si/(Si + {}^{[4]}Al)$]. If, as Volfinger et al. (1985) have suggested, the principal control on the incorporation of Cl in biotite is largely structural, then the incorporation of Cl into amphiboles may be controlled by the same parameters since the OH sites in amphibole and biotite are very similar.

These disparate hypotheses on the nature of Cl in micas and amphiboles, in addition to the recent suggestion by Munoz (1990) that Cl may not reside in the OH site, indicate that the controls on the incorporation of Cl into micas and amphiboles are poorly understood. This paper presents compositional data on a suite of halogen-bearing amphiboles from granulite-facies orthogneisses, and compositional variations among the amphiboles are used to evaluate constraints on the incorporation of Cl in amphiboles. Implications for constraints on metamorphic and magmatic fluid compositions will be addressed in a separate paper (Morrison and Valley, in preparation).

Petrology and general geology

Amphibole compositions were determined in eight samples from the Marcy anorthosite massif in the Adirondack Mountains of northern New York State (Fig. 1). Of the metaigneous rocks found in the highlands, the Marcy anorthosite massif is a dominant lithology (Fig. 1). The anorthosite massif was intruded to relatively shallow levels in the crust, by at least 1086 Ma, prior to the regional granulite facies metamorphism (Valley and O'Neil, 1982; McLelland et al., 1988). The Adirondack highlands were subsequently metamorphosed to peak granulite temperatures of 750 ± 50 °C and pressures of 7.5 ± 1 kbar during the Grenville Orogeny between 1070 and 1025 Ma (Bohlen et al., 1985; McLelland et al., 1988).

Anorthosite-series rocks of the Marcy massif include true anorthosite (>90% plagioclase), gabbroic anorthosite (10–22.5% mafic minerals), and anorthositic gabbro (22.5–35% mafic minerals). Also included, though volumetrically less significant, are late-stage mafic differentiates that range in composition to oxide-rich pyroxenite (up to 98% mafic minerals). Anorthosite-series rocks contain variable quantities of plagioclase phenocrysts ($\approx An_{45}$) with interstitial clinopyroxene, orthopyroxene, garnet, plagioclase, Fe-Ti oxide, iron sulfide, apatite, amphibole, and quartz. Minor amounts of retrograde minerals such as calcite, chlorite, and sericite occur in most samples and document the infiltration of postmetamorphic hydrothermal fluids (Morrison and Valley, 1988, 1991). Biotite is uncommon in anorthosite-series rocks, and when present it is also secondary.

The mineralogy of samples discussed in this paper is reported in Table 1. Amphibole textures are reported in Table 2. In anorthosites and gabbroic anorthosites, amphibole generally constitutes <2% of the rock by volume. Anorthositic gabbros and more mafic anorthosite-series rocks contain up to 10% amphibole. Three distinct textures characterize the occurrence of amphibole (Fig. 2). Amphibole occurs as coarse (1–2 mm across) equant to tabular intergrowths with pyroxene, plagioclase, and less commonly garnet (Fig. 2A). Amphibole also occurs as discrete rims around either pyroxene or Fe-Ti oxides (Fig. 2B). The rims range in width from 0.1 to 2.0 mm. Finally, inclusions of amphibole, 5–10 μm across, occur within plagioclase phenocrysts.

It is difficult to establish accurately the timing of amphibole equilibration or growth. The occurrence of amphibole as rims around pyroxene and Fe-Ti oxide (Fig. 2B) is classically interpreted to indicate postpeak metamorphic equilibration (Buddington, 1939), and it is likely that amphiboles in the anorthosite are also late metamorphic. The timing of equilibration of amphiboles with other textures, such as the lathlike intergrowths of amphibole with pyroxene, plagioclase, or garnet (Fig. 2A), is more difficult to interpret. It is possible that the different textures reflect discrete generations of amphibole (equilibrated at different temperatures). If this is correct, then temperature-sensitive compositional variations should correlate with textural occurrence. Neither halogen nor

Table 1. Sample mineralogy

Sample	Plag	Opx	Cpx	Ox	Ap	Amph	Gnt	Other	Retrograde
83-SR-4	X	X	X	X	X	X	X	Qt	Ser, Chl, Bi
83-RB-11	X	X	X	X		X		Qt	Ser, Chl, Bi
84-SR-8	X	X		X	X	X		Qt, Sf	Ser
84-SR-10I	X		X	X	X	X		Sf	Ser, Chl, Bi
SL-11Y	X	X	X	X		X		Sf	
83-AUS-20	X		X	X	X	X	X	Qt, Sf	Cc, Ser, Ep
84-SN-7	X		X	X	X	X	X	Qt, Sf	Cc, Ser, Chl
83-SR-1	X		X	X		X	X	Qt, Sf	Ser, Bi

Note: Abbreviations: Plag = plagioclase; Opx = orthopyroxene; Cpx = clinopyroxene; Ox = Fe-Ti oxides, ilmenite ± hematite ± magnetite; Ap = apatite; Amph = amphibole; Gnt = garnet; Qt = quartz; Sf = sulfides, pyrite ± pyrrhotite; Ksp = potassium feldspar; Bi = biotite; Ser = sericite; Chl = chlorite; Cc = calcite; Ep = epidote.

cation variations are directly related to textural variation; different textures are found within a single sample. Additionally, Cl-rich and Cl-poor amphiboles occur as both rims and lathlike intergrowths. For example, the amphibole in both 84-SR-8, analysis 1 and 83-SR-1, analysis 2 occurs as rims around Fe-Ti oxide. Except for a slight difference in color, the amphiboles are texturally indistinguishable, yet one contains 2.55 wt% Cl and the other contains 0.19 wt% Cl.

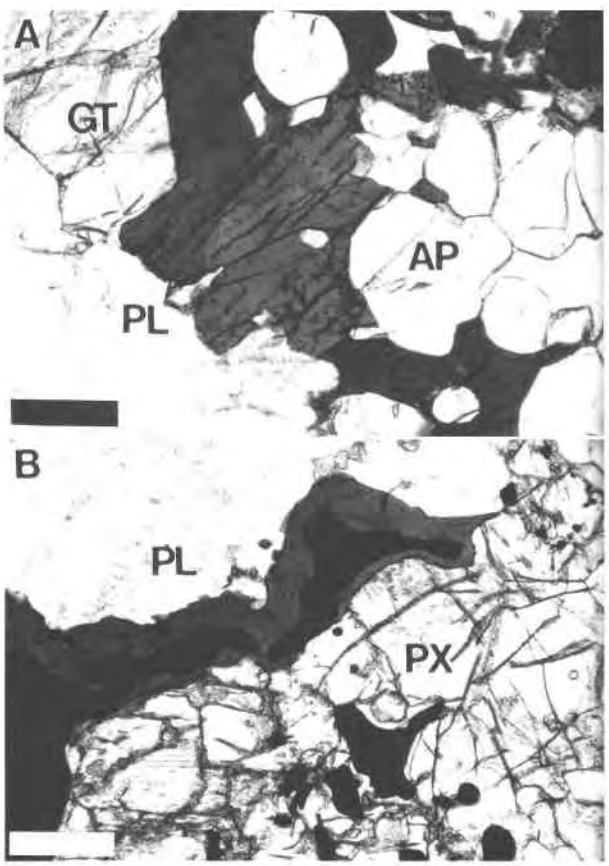

Fig. 2. Photomicrographs of amphibole textures. (**A**) Discrete amphibole grains adjacent to plagioclase (PL), garnet (GT), and apatite (AP). Scale bar = 0.4 mm. (**B**) Amphibole rims around Fe-Ti oxide, adjacent to pyroxene (PX) and plagioclase. Rims range in width from 2 mm down to 0.05 mm. Scale bar = 0.2 mm.

Apatite is a minor constituent ($\ll 1\%$) except in the oxide-rich, late-stage differentiates in which apatite may constitute up to 10% of the rock. Apatite usually occurs as equant or tabular subhedral grains. The apatites contain both F and Cl, but systematic correlations between amphibole and apatite compositions have not been observed. The significance of this observation will be discussed in a separate paper (Morrison and Valley, in preparation).

Analytical techniques

Electron microprobe analyses of all elements were conducted on an automated Cameca electron probe at the University of California at Los Angeles using wavelength dispersive PET, LiF, and RAP crystal spectrometers. Both natural and synthetic standards were used. A synthetic fluorphlogopite containing 9.02 wt% F was used as the

Table 2. Textural occurrence of amphibole

Sample, analysis	Texture
83-SR-4, 1	Discrete grain
83-SR-4, 2	Discrete grain, adjacent to Fe-Ti oxide
83-SR-4, 3	Discrete grain
83-RB-11, 1	Discrete grain
83-RB-11, 2	Discrete grain
83-RB-11, 3	Rim around Fe-Ti oxide, within 40 μm of oxide
83-RB-11, 4	Rim around Fe-Ti oxide, within 40 μm of oxide
84-SR-8, 1	Rim around Fe-Ti oxide
84-SR-8, 2	Discrete grain, adjacent to Fe-Ti oxide
84-SR-8, 3	Discrete grain, adjacent to Fe-Ti oxide
84-SR-10I, 1	Rim around Fe-Ti oxide
84-SR-10I, 2	Rim around Fe-Ti oxide
84-SR-10I, 3	Rim around Fe-Ti oxide
SL-11Y, 1	Discrete grain
SL-11Y, 2	Discrete grain
SL-11Y, 3	Discrete grain
83-AUS-20, 1	Discrete grain, adjacent to Fe-Ti oxide
83-AUS-20, 2	Discrete grain
83-AUS-20, 3	Discrete grain
83-AUS-20, 4	Discrete grain
83-AUS-20, 5	Discrete grain
84-SN-7, 1	Discrete grain
84-SN-7, 2	Discrete grain, intergrown with pyroxene
84-SN-7, 3	Discrete grain
83-SR-1, 1	Discrete grain, adjacent to Fe-Ti oxide
83-SR-1, 2	Rim around Fe-Ti oxide

standard for F. A barium-chlorapatite with 3.52 wt% Cl was used as the standard for Cl. All analyses were conducted with an accelerating potential of 15 keV. Great care was taken to determine whether volatilization of light elements, particularly F, occurred under these conditions. Using the synthetic fluorphlogopite standard, a 10-μm beam diameter, and a 0.010 μA sample current, total F counts over 10-s intervals were recorded for 300 s on a single spot. No decrease in counts was observed, so these conditions were used for subsequent analyses.

Amphibole formulas were normalized to 13 octahedral and tetrahedral cations (M1, M2, M3, and T sites), which assumes no octahedral or tetrahedral vacancies but permits vacancies in the A and M4 sites. Fe^{3+} was calculated from charge balance using the relation $Fe^{3+} = {}^{[4]}Al - {}^{[6]}Al - 2Ti - {}^{[A]}Na - {}^{[A]}K + {}^{[M4]}Na$, and OH was calculated by difference, assuming Cl + F + OH = 2. A comparison with the formula derived from the 24-anion (O, OH, F, Cl) normalization was made to evaluate the importance of the normalization scheme. The anion normalization results in higher average cations and anions pfu, with the most significant difference in Si. However, the important halogen-cation correlations are observed in formulas from either normalization scheme. The A site vacancies are, on average, smaller when normalized to 24 anions.

Results

Amphibole compositions from anorthosite-series rocks are listed in Table 3. Compositions are listed for several texturally distinct, discrete grains within a given sample. In the majority of samples, between five and seven spots were analyzed per grain. Where grain size prevented this, two to four spots per grain were analyzed.

Two distinct groups of amphibole can be delineated on the basis of Cl content: a Cl-rich group, which contains between 3.00 and 1.84 wt% Cl, and a Cl-poor group, which contains between 0.47 and 0.02 wt% Cl. Following Leake's (1978) classification, all of the Cl-rich amphiboles are ferropargasite or chlor-ferropargasite. The Cl-poor group are all ferropargasitic hornblendes. It should be noted that Leake's classification is defined primarily for amphiboles normalized to 24 anions (O, OH, F, Cl), and in the present study amphiboles have been normalized to 13 tetrahedral and octahedral cations. Normalization to 24 anions shifts a few of the ferropargasitic hornblendes into Leake's ferro-edenitic hornblende field.

Zonation has been detected in amphiboles that touch Fe-Ti oxides, but zonation is limited to the outer 40–50 μm. This zonation is documented in sample 83-RB-11; amphibole within 40–50 μm of Fe-Ti oxides (83-RB-11, analyses 3 and 4) is depleted in Fe and Ti relative to the interior portions of amphibole grains (83-RB-11, analyses 1 and 2). This Fe-Ti depletion is interpreted as resulting from retrograde exchange with the adjacent Fe-Ti oxide. Great care was taken to avoid the outermost rims of amphiboles in contact with Fe-Ti oxides. Note that the reequilibrated compositions of 83-RB-11 (analyses 3 and 4) have not been plotted on the following figures.

Cl and F in amphiboles

A number of correlations exist between cation and halogen compositions. In Figure 3, relations between X_{Mg} and wt% Cl and wt% F are shown. Cl-rich amphiboles are plotted as solid squares, and Cl-poor amphiboles are plotted as open squares in all figures. Both Cl-rich and Cl-poor amphiboles show an inverse correlation between X_{Mg} and wt% Cl, although linear regression of the two groups indicates that the correlation is significantly stronger among the Cl-poor amphiboles ($r^2 = 0.85$) than among the Cl-rich amphiboles ($r^2 = 0.35$). Thus, Mg-Cl avoidance is clearly evident in the Cl-poor amphiboles, and it probably represents the principal control on Cl incorporation in amphiboles that contain relatively minor amounts of Cl (e.g., <1 wt% Cl). However, among the Cl-rich amphiboles, Mg-Cl avoidance is not strongly established. The general trend of the Cl-rich data is broadly similar to that of the Cl-poor data (slopes of -5.2 ± 2.0 and -2.4 ± 0.4, respectively). The weak correlation between X_{Mg} and wt% Cl in the Cl-rich amphiboles ($r^2 = 0.35$) suggests that Mg-Cl avoidance is not a dominant control on Cl incorporation in amphiboles with significant amounts of Cl (e.g., >1.5 wt% Cl). The significance of this difference will be discussed in more detail below.

Figure 3B illustrates the opposing behavior of F relative to Cl. F contents of the Cl-rich amphiboles show a broadly positive but weak correlation ($r^2 = 0.39$) with increasing X_{Mg} (or decreasing X_{Fe}) as do the Cl-poor amphiboles ($r^2 = 0.43$). Fe-F avoidance is not well developed among the amphiboles.

Equilibration conditions

In order to evaluate the significance of the compositional variations observed in Figure 3, it is important to establish whether the amphiboles equilibrated under the same temperature and fluid conditions. It is possible that the difference in Cl content between the Cl-rich and Cl-poor amphiboles could reflect equilibration at significantly different temperatures but broadly similar fluid conditions. Extensive thermometry has been conducted throughout the Adirondack highlands that indicates that the Marcy anorthosite massif was metamorphosed at peak temperatures between 725 and 800 °C (Bohlen et al., 1985). Differences in peak metamorphic temperatures among the samples were probably not greater than 50 or 75 °C. The Marcy anorthosite is confined within the Adirondack highlands, so all samples are likely to have undergone very similar cooling and uplift histories.

If the distinct amphibole textures reflect equilibration at different temperatures, e.g., earlier, higher temperature equilibration of discrete grains and lathlike intergrowths followed by late-stage, lower temperature equilibration of the amphibole rims, then compositions should correlate with texture. As discussed earlier, examination of the data in Tables 2 and 3 indicates that no such correlations are present, with the exception of sample 83-RB-11 in which retrograde exchange of Fe and Ti are observed at the outermost rim of amphibole in contact with oxide. Rim-

TABLE 3. Electron microprobe analyses of amphiboles from the Marcy anorthosite massif

Sample	83-SR-4	83-SR-4	83-SR-4	83-RB-11	83-RB-11	83-RB-11	83-RB-11	84-SR-8	84-SR-8	84-SR-8	84-SR-10I	84-SR-10I	84-SR-10I
Analysis	1	2	3	1	2	3	4	1	2	3	1	2	3
SiO_2	37.88	37.92	38.02	39.30	39.33	39.73	39.52	37.94	38.19	38.05	37.96	37.75	37.94
TiO_2	1.91	1.48	1.79	2.51	2.47	1.78	1.81	1.49	1.73	1.63	1.61	1.54	1.63
Al_2O_3	12.60	12.76	12.53	13.25	13.33	14.03	14.14	13.29	13.09	12.99	13.03	13.62	13.19
Fe_2O_3	2.39	3.06	3.12	1.09	1.80	2.99	3.27	2.85	3.18	3.25	4.26	4.03	2.74
FeO	20.46	19.91	19.70	17.15	16.39	13.03	12.24	17.82	17.42	17.81	17.77	16.92	18.93
MnO	0.09	0.05	0.10	0.14	0.15	0.10	0.09	0.12	0.17	0.21	0.14	0.11	0.16
MgO	5.45	5.74	5.88	8.25	8.44	10.00	10.03	6.89	7.05	6.69	6.26	6.77	6.30
CaO	11.31	11.49	11.35	11.56	11.58	11.86	11.77	11.49	11.40	11.32	11.08	11.31	11.39
Na_2O	0.99	1.05	1.18	1.21	1.17	0.95	0.75	1.02	1.09	1.06	1.17	1.03	1.09
K_2O	3.07	3.06	2.89	3.15	3.11	3.22	3.16	3.30	3.16	3.09	3.02	3.17	3.33
H_2O	1.13	1.12	1.18	1.11	1.09	0.94	1.01	0.90	0.97	0.95	1.03	0.91	0.83
F	0.33	0.23	0.30	0.53	0.57	1.00	0.84	0.55	0.61	0.48	0.43	0.49	0.66
Cl	2.32	2.63	2.27	2.32	2.33	2.23	2.20	2.93	2.55	2.85	2.60	2.99	3.00
Total	99.93	100.50	100.40	101.57	101.76	101.86	100.83	100.59	100.61	100.38	100.36	100.64	101.19
$O \equiv F, Cl$	0.66	0.69	0.64	0.75	0.77	0.92	0.85	0.89	0.83	0.85	0.77	0.88	0.96
Total	99.27	99.81	99.76	100.82	100.99	100.94	99.98	99.70	99.78	99.53	99.59	99.76	100.23
					Normalized to 13 tetrahedral and octahedral cations								
Si	6.029	6.020	6.022	6.048	6.028	6.006	6.006	5.987	5.996	6.007	5.989	5.936	5.998
$^{[4]}Al$	1.956	1.980	1.978	1.952	1.972	1.944	1.994	2.013	2.004	1.993	2.011	2.064	2.012
$^{[6]}Al$	0.414	0.409	0.362	0.452	0.436	0.506	0.539	0.459	0.419	0.424	0.412	0.461	0.443
Ti	0.229	0.177	0.213	0.290	0.285	0.202	0.207	0.177	0.204	0.194	0.191	0.182	0.193
Fe^{3+}	0.286	0.366	0.372	0.128	0.207	0.341	0.375	0.339	0.377	0.386	0.506	0.477	0.325
Mg	1.296	1.358	1.388	1.892	1.928	2.253	2.272	1.620	1.650	1.574	1.472	1.587	1.482
Fe^{2+}	2.763	2.648	2.651	2.220	2.125	1.684	1.596	2.389	2.328	2.395	2.401	2.279	2.535
Mn	0.012	0.007	0.013	0.018	0.019	0.013	0.012	0.016	0.023	0.028	0.019	0.015	0.021
$^{[M4]}Na$	0.066	0.045	0.074	0.094	0.098	0.079	0.083	0.057	0.082	0.085	0.127	0.094	0.074
$^{[A]}Na$	0.24	0.278	0.289	0.267	0.249	0.200	0.137	0.255	0.250	0.239	0.231	0.220	0.260
Ca	1.934	1.955	1.926	1.906	1.902	1.921	1.917	1.943	1.918	1.915	1.873	1.906	1.926
K	0.625	0.620	0.602	0.618	0.608	0.621	0.613	0.664	0.633	0.642	0.608	0.636	0.671
OH	1.206	1.177	1.241	1.137	1.119	0.951	1.029	0.942	1.019	0.998	1.090	0.959	0.869
F	0.167	0.115	0.150	0.258	0.276	0.478	0.404	0.274	0.303	0.240	0.215	0.244	0.329
Cl	0.627	0.708	0.609	0.605	0.605	0.571	0.567	0.784	0.678	0.762	0.695	0.797	0.802
X_{Mg}	0.259	0.272	0.278	0.378	0.386	0.451	0.454	0.324	0.330	0.315	0.294	0.317	0.296
$Si/(Si + {}^{[4]}Al)$	0.756	0.753	0.753	0.751	0.754	0.751	0.751	0.748	0.750	0.751	0.749	0.742	0.750
X_{Cl}	0.314	0.354	0.305	0.285	0.303	0.286	0.200	0.392	0.399	0.381	0.348	0.399	0.401
X_F	0.084	0.058	0.075	0.221	0.239	0.239	0.017	0.137	0.152	0.120	0.108	0.122	0.165
X_{OH}	0.603	0.589	0.621	0.495	0.560	0.476	0.783	0.471	0.510	0.499	0.545	0.480	0.431
$\log(X_F/X_{Cl})$	−0.573	−0.786	−0.609	−0.371	−0.342	−0.078	0.711	−0.457	−0.348	−0.502	−0.508	−0.515	−0.386

TABLE 3—*Continued*

Sample	SL-11Y	SL-11Y	SL-11Y	83-AUS-20	83-AUS-20	83-AUS-20	83-AUS-20	83-AUS-20	84-SN-7	84-SN-7	84-SN-7	83-SR-1	83-SR-1
Analysis	1	2	3	1	2	3	4	5	1	2	3	1	2
SiO_2	39.51	39.11	39.35	40.85	41.27	40.73	40.70	40.80	42.75	43.03	42.81	41.73	41.83
TiO_2	2.41	2.98	2.95	1.83	2.24	2.40	2.29	2.54	2.90	2.34	2.37	1.69	1.64
Al_2O_3	13.26	12.96	12.94	13.54	12.67	12.86	12.98	12.80	12.14	12.09	12.53	12.82	12.90
Fe_2O_3	1.03	0.18	0.93	2.84	1.93	1.77	2.06	1.87	1.18	2.39	2.17	3.71	3.40
FeO	16.12	17.55	16.83	16.1	17.79	18.38	18.07	17.90	14.00	12.77	11.98	13.68	13.68
MnO	0.13	0.13	0.31	0.06	0.06	0.05	0.09	0.06	0.12	0.11	0.08	0.03	0.06
MgO	8.73	8.17	8.41	8.13	7.77	7.46	7.39	7.38	10.69	11.02	11.38	9.64	9.84
CaO	11.49	11.32	11.44	11.65	11.57	11.62	11.50	11.40	11.80	11.74	11.73	11.61	11.78
Na_2O	2.00	1.93	1.95	1.12	1.23	1.27	1.24	1.29	1.28	1.46	1.35	1.17	1.13
K_2O	1.82	2.13	2.02	2.29	2.24	2.30	2.37	2.23	1.97	1.67	1.87	2.25	2.30
H_2O	1.22	1.12	1.28	1.79	1.81	1.78	1.79	1.77	1.74	1.89	1.90	1.77	1.69
F	0.61	0.69	0.43	0.24	0.16	0.16	0.14	0.17	0.59	0.29	0.27	0.40	0.58
Cl	1.74	1.90	1.84	0.36	0.44	0.43	0.47	0.43	0.02	0.02	0.20	0.19	0.18
Total	100.07	100.17	100.68	100.80	101.18	101.21	101.09	100.64	101.18	100.69	100.46	100.69	101.01
$O \equiv F, Cl$	0.65	0.72	0.60	0.18	0.17	0.16	0.17	0.17	0.25	0.13	0.12	0.21	0.29
Total	99.42	99.45	100.08	100.62	101.01	101.05	100.92	100.47	100.93	100.69	100.34	100.48	100.72
Normalized to 13 tetrahedral and octahedral cations													
Si	6.084	6.071	6.056	6.161	6.237	6.178	6.178	6.212	6.317	6.340	6.308	6.232	6.231
$^{[4]}Al$	1.916	1.929	1.944	1.839	1.763	1.822	1.823	1.788	1.683	1.660	1.692	1.768	1.769
$^{[6]}Al$	0.492	0.443	0.403	0.568	0.495	0.477	0.500	0.509	0.432	0.439	0.485	0.489	0.496
Ti	0.279	0.348	0.341	0.208	0.255	0.274	0.261	0.291	0.322	0.259	0.263	0.190	0.184
Fe^{3+}	0.119	0.021	0.107	0.322	0.219	0.202	0.235	0.163	0.131	0.265	0.241	0.416	0.381
Mg	2.004	1.890	1.929	1.827	1.750	1.686	1.672	1.675	2.354	2.420	2.499	2.146	2.184
Fe^{2+}	2.089	2.280	2.179	2.067	2.274	2.354	2.320	2.354	1.745	1.603	1.503	1.755	1.747
Mn	0.017	0.017	0.040	0.008	0.008	0.006	0.012	0.008	0.015	0.014	0.010	0.004	0.008
$^{[M4]}Na$	0.104	0.117	0.114	0.117	0.126	0.111	0.130	0.140	0.132	0.147	0.148	0.142	0.120
$^{[A]}Na$	0.493	0.464	0.468	0.210	0.234	0.262	0.235	0.260	0.235	0.270	0.238	0.197	0.207
Ca	1.896	1.883	1.886	1.883	1.874	1.889	1.870	1.876	1.868	1.853	1.852	1.858	1.880
K	0.358	0.422	0.397	0.441	0.432	0.445	0.459	0.437	0.371	0.314	0.352	0.429	0.437
OH	1.249	1.161	1.316	1.794	1.811	1.812	1.812	1.807	1.719	1.860	1.869	1.763	1.682
F	0.297	0.339	0.204	0.114	0.076	0.077	0.067	0.082	0.276	1.350	0.126	0.189	0.273
Cl	0.454	0.500	0.480	0.092	0.113	0.111	0.121	0.111	0.005	0.005	0.005	0.048	0.045
X_{Mg}	0.401	0.378	0.386	0.365	0.350	0.337	0.334	0.335	0.471	0.484	0.500	0.429	0.437
$Si/(Si + {}^{[4]}Al)$	0.761	0.759	0.757	0.770	0.780	0.772	0.772	0.777	0.790	0.793	0.789	0.779	0.777
X_{Cl}	0.227	0.250	0.240	0.046	0.057	0.056	0.061	0.056	0.003	0.003	0.003	0.024	0.023
X_F	0.149	0.170	0.102	0.057	0.038	0.039	0.034	0.041	0.138	0.675	0.063	0.095	0.137
X_{OH}	0.625	0.581	0.658	0.897	0.906	0.906	0.906	0.904	0.860	0.930	0.935	0.882	0.841
$\log(X_F/X_{Cl})$	−0.183	−0.167	−0.372	0.093	−0.176	−0.157	−0.254	−0.135	1.663	1.355	1.322	0.598	0.775

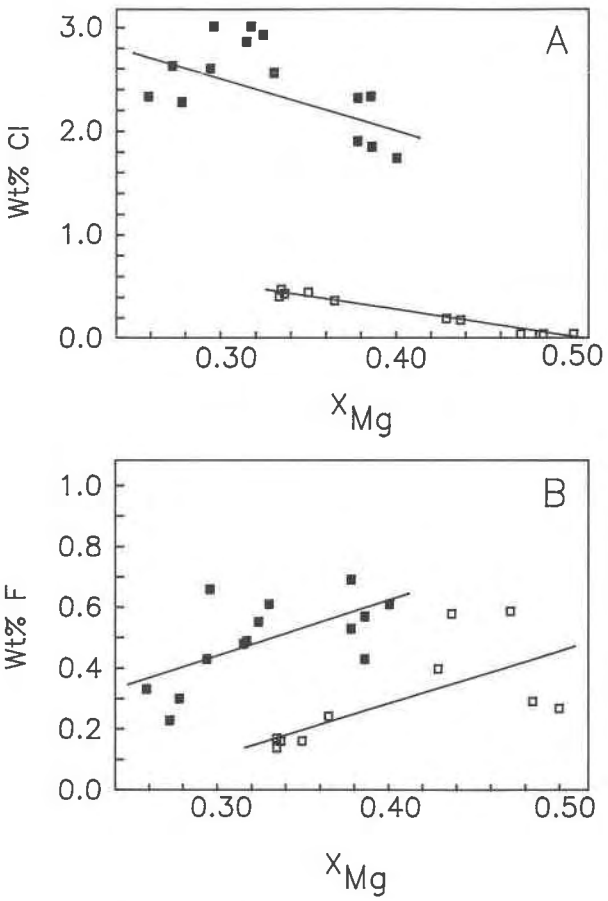

Fig. 3. (**A**) Relations between X_{Mg} and wt% Cl in 24 amphiboles (Table 3). Solid squares are Cl-rich amphiboles, and open squares are Cl-poor amphiboles. The solid lines define the best-fit equation for each group of amphiboles, calculated with a linear least-squares regression. The Cl-poor amphiboles are strongly inversely correlated ($r^2 = 0.85$), illustrating Mg-Cl avoidance (see text). The Cl-rich amphiboles have the same overall X_{Mg} vs. wt% Cl trend as the Cl-poor amphiboles but are not as strongly correlated ($r^2 = 0.35$). (**B**) Relations between X_{Mg} and wt% F in 24 amphiboles (Table 3). Symbols are the same as in **A**. Correlations between X_{Mg} and F are not strongly developed but do illustrate the opposing behavior of F relative to Cl.

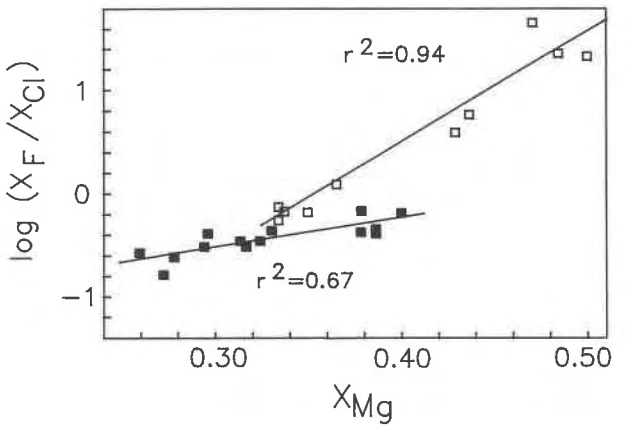

Fig. 4. Plot of X_{Mg} vs. $\log(X_F/X_{Cl})$ for Cl-rich (solid squares) and Cl-poor (open squares) amphiboles. The Cl-poor amphiboles are strongly correlated ($r^2 = 0.94$), which is interpreted to indicate that they have equilibrated at the same temperature with a fluid of constant f_{HF}/f_{HCl}. A significant but weaker correlation characterizes the Cl-rich amphiboles ($r^2 = 0.67$). The substantial difference in slope between the Cl-rich and Cl-poor data (2.8 ± 0.6 and 10.6 ± 1.0, respectively) is interpreted to indicate that compositional constraints other than X_{Mg} differentially affect the incorporation of Cl in Cl-rich vs. the Cl-poor amphiboles.

ming textures, in which amphibole surrounds both oxide and pyroxene, are observed among both Cl-rich and Cl-poor amphiboles. Thus, the distinct textures do not appear to reflect discrete generations of amphibole; if textures are a reliable indicator of timing of equilibration, then it is reasonable to conclude that amphibole equilibration was broadly synchronous in terms of time and therefore temperature.

The large difference in Cl contents between the Cl-rich and Cl-poor amphiboles may be the result of equilibration with significantly different fluid compositions. It is possible to evaluate this, and the previous interpretation that the amphiboles equilibrated at the same temperature, by examining relations between $\log(X_F/X_{Cl})$ and X_{Mg}. Munoz and Swenson (1981) have shown that biotite with variable X_{Mg} that equilibrated with a fluid of constant (f_{HF}/f_{HCl}) at the same temperature should plot as a straight line on a $\log(X_F/X_{Cl})$ vs. X_{Mg} plot. This is true provided X_{Mg} is the principal compositional constraint on the incorporation of Cl. In Figure 4, significant correlations between $\log(X_F/X_{Cl})$ and X_{Mg} for both Cl-rich and Cl-poor amphiboles are observed. Two important aspects of the data in Figure 4 are (1) the difference in extent of correlation between the Cl-rich and Cl-poor amphiboles ($r^2 = 0.67$ and 0.94, respectively) and (2) the difference in slope (2.8 ± 0.6 and 10.6 ± 1.0, respectively). The difference in slope between Cl-rich and Cl-poor amphiboles suggests that (1) parameters other than X_{Mg} have differentially affected the Cl-rich vs. Cl-poor amphiboles and (2) among the Cl-rich amphiboles Cl = F = OH exchange is substantially nonideal ($a \neq X$). To evaluate the significance of these differences, it is necessary to examine the construction of the $\log(X_F/X_{Cl})$ vs. X_{Mg} diagram in more detail.

Exchange of Cl or F for OH between amphibole or biotite and a coexisting fluid or silicate melt may be modeled by the reactions

$$AB(OH) + HCl = AB(Cl) + H_2O \quad (1)$$

$$AB(OH) + HF = AB(F) + H_2O \quad (2)$$

where AB represents amphibole or biotite. The equilibrium constants for these reactions, K_1 and K_2, are given by

$$\log K_1 = \log(a_{Cl}/a_{OH})_{Amph,Biot} + \log(a_{H_2O}/a_{HCl})_{Fluid} \quad (3)$$

$$\log K_2 = \log(a_F/a_{OH})_{Amph,Biot} + \log(a_{H_2O}/a_{HF})_{Fluid}. \quad (4)$$

By assuming ideal mixing of Cl, F, and OH on the OH site (a significant assumption that will be reevaluated below) and converting activities of fluid species to fugacities, the relations become

$$\log K_1 = \log(X_{Cl}/X_{OH})_{Amph,Biot} + \log(f_{H_2O}/f_{HCl})_{Fluid} \quad (5)$$

$$\log K_2 = \log(X_F/X_{OH})_{Amph,Biot} + \log(f_{H_2O}/f_{HF})_{Fluid}. \quad (6)$$

If the equilibrium constants for these reactions were known, it would be possible to calculate the ratio of fluid species fugacities that existed during equilibration.

Since OH is not measured directly, X_{OH} is subject to substantial uncertainty and can be eliminated by subtracting Equation 1 from Equation 2, yielding

$$AB(Cl) + HF = AB(F) + HCl. \quad (7)$$

The equilibrium constant for Reaction 7 is

$$\log K = \log(X_F/X_{Cl})_{Amph,Biot} + \log(f_{HF}/f_{HCl})_{Fluid}. \quad (8)$$

This formulation of the equilibrium constant is useful because it enables evaluation of differences in the ratio of f_{HF}/f_{HCl} from X_{Cl} and X_F, which can be determined with much greater accuracy than X_{OH}.

Munoz and Swenson (1981) argued that it was reasonable to recast the temperature and compositional dependance of log K for Equations 1 and 2 (or 7) as

$$\log K = A/T + BX_{Mg} + C \quad (9)$$

where A, B, and C were derived from experimentally determined Arrhenius relations. Combining this with Equation 8 yields

$$\log(X_F/X_{Cl})_{Amph,Biot} = BX_{Mg} + [\log(f_{HF}/f_{HCl})_{Fluid} + A/T + C]. \quad (10)$$

At a given T and $(f_{HF}/f_{HCl})_{Fluid}$, the terms enclosed in brackets in Equation 10 are constant, and amphiboles or biotite with variable X_{Mg}'s should plot as a straight line on a $\log(X_F/X_{Cl})$ vs. X_{Mg} plot. The slope of the line (B) reflects the effect of X_{Mg} on halogen incorporation for Reaction 7. Thus, simple interpretations can only be derived from a $\log(X_F/X_{Cl})$ vs. X_{Mg} plot provided X_{Mg} is the principal compositional control on halogen incorporation.

If all constraints on the incorporation of Cl and F into Cl-rich vs. Cl-poor amphiboles except fluid composition were equal, then $\log(X_F/X_{Cl})$ vs. X_{Mg} data should define two linear arrays with similar slopes, and the separation between the two arrays would reflect the variable f_{HF}/f_{HCl} of the fluid. If all constraints among each group except temperature were equal, the data would also define two linear arrays with the same slope, the separation reflecting the effect of temperature on halogen-mineral partitioning.

In Figure 4, the correlation between $\log(X_F/X_{Cl})$ and X_{Mg} among the Cl-poor amphiboles is very strong (r^2 = 0.94) and is interpreted as evidence that the Cl-poor amphiboles equilibrated at the same temperature and $(f_{HF}/f_{HCl})_{Fluid}$. Munoz and Swenson (1981) have noted that equilibration between mineral and fluid at variable temperatures or $(f_{HF}/f_{HCl})_{Fluid}$ ratios will result in "incoherent scatter" on a $\log(X_F/X_{Cl})$ vs. X_{Mg} plot because of the strong temperature and compositional dependence of the equilibrium constant for Reactions 1 and 2 (or 7).

Among the 14 Cl-rich amphiboles, the correlation is not as strong (r^2 = 0.67) but is still significant. As discussed above, a strong correlation on a $\log(X_F/X_{Cl})$ vs. X_{Mg} plot is expected at constant T and $(f_{HF}/f_{HCl})_{Fluid}$ provided X_{Mg} is the dominant control on halogen incorporation. The weak correlation among the Cl-rich amphiboles in Figure 4 follows directly from the weak correlation between X_{Mg} and Cl shown in Figure 3A.

The absence of a strong correlation between Cl and X_{Mg} among the Cl-rich amphiboles is likely due to either (1) equilibration at variable temperatures, (2) equilibration at variable fluid compositions, or (3) compositional constraints on the incorporation of Cl other than X_{Mg}.

Cation-halogen systematics

If cation variations other than X_{Mg} exert control on halogen compositions, then systematic cation-halogen variations should exist. The data have been carefully evaluated, and a number of significant correlations exist. If, as discussed above, the weak correlation between X_{Mg} and Cl among the Cl-rich amphiboles were due to equilibration at variable $(f_{HF}/f_{HCl})_{Fluid}$ or temperature, then one would not expect strong cation-halogen correlations. One would be required to argue that any correlations, such as those shown in Figures 5–7 (and discussed below), were fortuitous. This is not considered likely; thus, the strong cation-halogen correlations are interpreted to indicate that the Cl-rich amphiboles equilibrated at similar $(f_{HF}/f_{HCl})_{Fluid}$ and temperatures.

In Figure 5A, the variation in Cl is plotted against the mole fraction of Si in the tetrahedral site [X_{Si} = Si/(Si + $^{[4]}$Al)]. In Figure 5B, F is plotted vs. X_{Si}, showing no correlation. The data for both Cl-rich and Cl-poor amphiboles show good negative correlations between X_{Si} and Cl. The most dramatic correlation occurs among the Cl-rich group, in which small changes in Si content correspond to large changes in Cl.

The reason for this correlation is unclear. Volfinger et al. (1985) have predicted that for a constant fluid composition and temperature, an increase in X_{Si} will result in an increase in the Cl content of a mica or amphibole. Data in Figure 5A contradict this prediction.

In Figure 6, relations between Cl content and A site

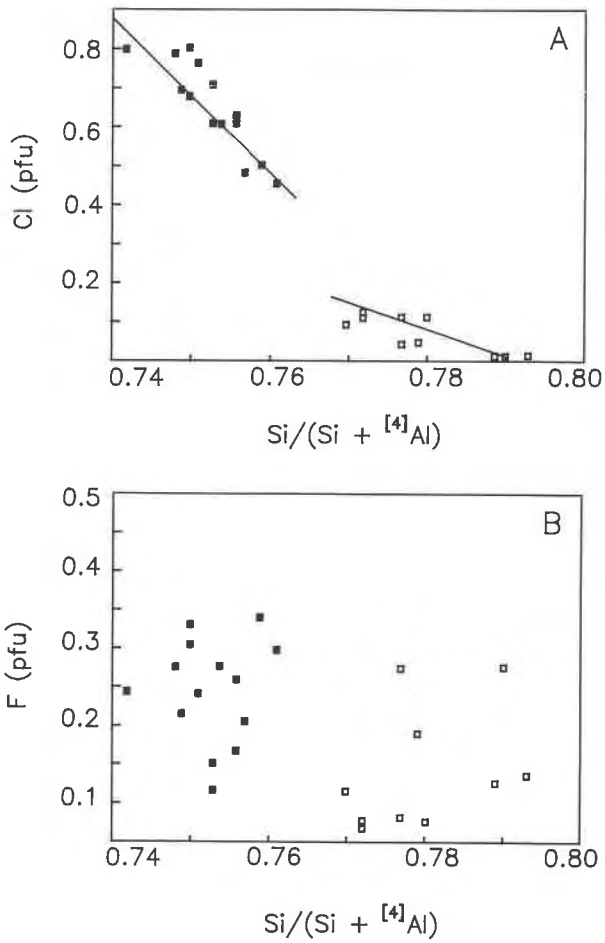

Fig. 5. (**A**) Plot of X_{Si} vs. Cl. The Cl-rich amphiboles (solid squares) have distinctly lower X_{Si} values than do the Cl-poor amphiboles (open squares). An inverse correlation between $^{[4]}$Si and Cl characterizes both Cl-rich and Cl-poor amphiboles. (**B**) Relations between X_{Si} and F indicate that F contents vary independently of X_{Si}.

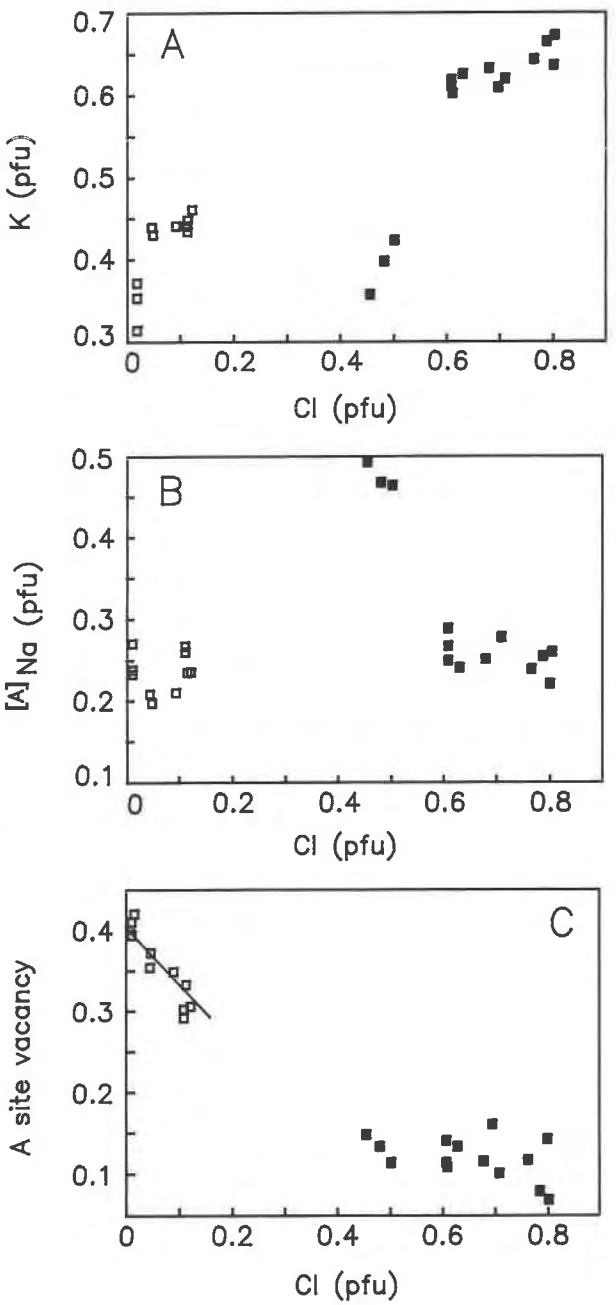

Fig. 6. Relations between Cl content and A site occupancy. (**A**) Both Cl-rich (solid squares) and Cl-poor amphiboles (open squares) are positively correlated with K. (**B**) $^{[A]}$Na does not show any systematic variations with Cl content. (**C**) A strong inverse linear relation between A site vacancy (= 1 − $^{[A]}$Na − K) and Cl content exists among Cl-poor amphiboles (r^2 = 0.89). In all Cl-rich amphiboles, the A site is virtually full.

occupancy are plotted. Figure 6A illustrates the relation between K and Cl contents; positive correlations exist among both Cl-rich (r^2 = 0.76) and Cl-poor (r^2 = 0.72) amphiboles. In the Cl-rich group, one rock sample contains significantly less K than the others. This sample, SL-11Y, is a more mafic rock, and the relative depletion in K is accompanied by an enrichment in $^{[A]}$Na, which is illustrated in Figure 6B. With the exception of sample SL-11Y, the $^{[A]}$Na of the Cl-rich and Cl-poor group are indistinguishable.

When Cl content is plotted against A site vacancy (= 1 − K − $^{[A]}$Na), a strong inverse correlation is observed among the Cl-poor group (r^2 = 0.89), and a strong distinction between the Cl-rich and Cl-poor groups emerges (Fig. 6C). Among the Cl-rich amphiboles, the A site is virtually full. It is important to note that this is not simply the result of high K contents. Sample SL-11Y, which is relatively depleted in K, is relatively enriched in Na, and the Na fills the A site to the same extent as K fills the site in the other Cl-rich amphiboles. The association between an essentially full A site and high Cl contents suggests that A site occupancy may exert some control on Cl content.

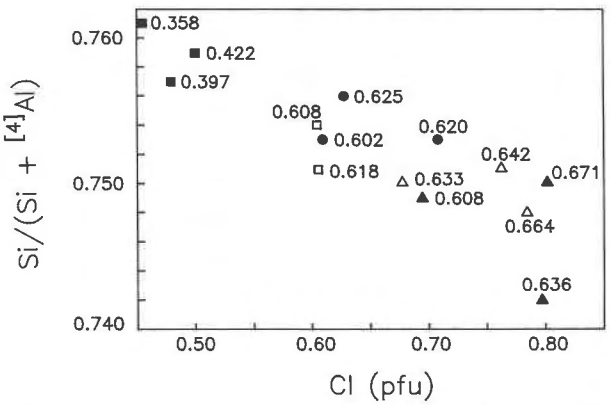

Fig. 7. Relations between Cl content and X_{Si} for the 14 Cl-rich amphiboles. Also plotted are K contents for each amphibole. Symbols: solid squares = SL-11Y; open squares = 83-RB-11; solid circles = 83-SR-4; open triangles = 84-SR-8; closed triangles = 84-SR-10I.

Additional insight into the relative importance of tetrahedral and A site occupancy on Cl content is gained by evaluating within sample variation. In Figure 7, relations between X_{Si} and Cl are plotted for the Cl-rich amphiboles. The K content of each amphibole is also plotted on Figure 7. At a given X_{Si} within a sample, increased amounts of Cl correlate with higher K contents. For example, in sample 83-SR-4, which is plotted as solid circles, the increase in Cl from 0.609 to 0.708 is accompanied by an increase in K from 0.602 to 0.620 at constant X_{Si} (0.753). Similarly, in sample 84-SR-8 at an X_{Si} = 0.750 and 0.751 (open triangles), the increase in Cl from 0.678 to 0.762 is accompanied by an increase in K from 0.633 to 0.642. In light of these multiple cation-halogen correlations, it is not surprising that Mg-Cl avoidance is only weakly established among the Cl-rich amphiboles.

Conclusions

In order to interpret accurately the compositional constraints on the incorporation of Cl and F into amphiboles, experimental data on the partitioning of Cl, F, and OH as a function of temperature, halogen acid species fugacity (f_{HF}, f_{HCl}), and composition (e.g., X_{Mg}, X_{Si}, A site occupancy) are required. Additionally, detailed structural refinements of both halogen-bearing and halogen-rich amphiboles will be necessary to resolve the nature of crystal chemical constraints that arise from local charge balance or cation site occupancy as they cannot be resolved from amphibole formulas derived by normalization of electron microprobe data. However, in the absence of experimental data, it may still be possible to draw some conclusions concerning halogen incorporation in amphiboles from compositions of natural samples, but one must recognize that the conclusions are dependent upon assumptions regarding the temperature and fluid composition.

If the Cl-rich and Cl-poor amphiboles equilibrated at the same temperature and if each group equilibrated with a fluid of constant f_{HF}/f_{HCl}, then it is possible to conclude the following about the incorporation of Cl in amphibole: In the presence of extremely Cl-rich fluids, X_{Si} and A site occupancy (particularly X_K) are stronger controls on Cl incorporation than is X_{Mg}. In the presence of relatively Cl-poor fluids, X_{Mg} is the predominant compositional control on the incorporation of Cl.

The strong inverse correlation between Si and Cl contents suggests that tetrahedral site occupancy may have important controls on the incorporation of Cl, particularly among the Cl-rich amphiboles. However, the nature of this relation is not well understood. Volfinger et al. (1985) have predicted that decreasing amounts of Si should result in increased distortion of the pseudohexagonal ring of tetrahedra, enabling increased amounts of Cl to fit in the OH site. The present data show the opposite trend and indicate that occupancy of the tetrahedral site by highly charged silica ions hinders the incorporation of Cl.

The correlations between A site occupancy (particularly X_K) and Cl content suggest that A site cations influence the incorporation of Cl in the OH site. Since the A site lies essentially "above" the OH site, it is possible that the $K^+ \cdots Cl^-$ approach may be energetically favored over the $K^+ \cdots H^+$-O^{2-} approach (i.e., $K^+ \cdots OH^-$) if Cl is available.

These results indicate that caution must be used when applying experimental mineral-fluid Cl = F = OH partitioning data to natural, Cl-rich amphiboles.

Acknowledgments

Funding for electron microprobe analyses was provided by a grant from the USC Faculty Research and Innovation Fund. Microprobe analyses were conducted at UCLA, and the assistance of Bob Jones is gratefully acknowledged. Jim Munoz and Lawford Anderson provided helpful reviews.

References cited

Bohlen, S.R., Valley, J.W., and Essene, E.J. (1985) Metamorphism in the Adirondacks I. Petrology, pressure, and temperature. Journal of Petrology, 26, 971–992.

Boudreau, A.E., Mathez, E.A., and McCallum, I.S. (1986) Halogen geochemistry of the Stillwater and Bushveld complexes: Evidence for transport of the platinum-group elements by Cl-rich fluids. Journal of Petrology, 27, 967–986.

Buddington, A.F. (1939) Adirondack igneous rocks and their metamorphism. Geological Society of America Memoir 7, 354 p.

Korzhinskiy, M.A. (1981) Apatite solid solutions as indicators of the fugacity of HCl and HF in hydrothermal fluids. Geochemistry International, 18, 44–60.

Leake, B.E. (1978) Nomenclature of amphiboles. Canadian Mineralogist, 16, 501–520.

McLelland, J., Chiarenzelli, J., Whitney, P., and Isachsen, Y. (1988) U-Pb zircon geochronology of the Adirondack Mountains and implications for their geologic evolution. Geology, 16, 920–924.

Mora, C.I., and Valley, J.W. (1989) Halogen-rich scapolite and biotite: Implications for metamorphic fluid-rock interaction. American Mineralogist, 74, 721–737.

Morrison, J., and Valley, J.W. (1988) Post-granulite facies fluid infiltration in the Adirondack Mountains. Geology, 16, 514–518.

——— (1991) Retrograde fluids in granulites: Stable isotope evidence of fluid migration. Journal of Geology, 99, 559–570.

Munoz, J.L. (1984) F-OH and Cl-OH exchange in micas with applications to hydrothermal ore deposits. In Mineralogical Society of America Reviews in Mineralogy, 13, 469–493.

——— (1990) F and Cl contents of hydrothermal biotites: A re-evaluation. Geological Society of America Abstracts with Programs, 22, A135.

Munoz, J.L., and Ludington, S.D. (1974) Fluoride-hydroxyl exchange in synthetic muscovite and its application to muscovite-biotite assemblages. American Mineralogist, 62, 304–308.

——— (1977) Fluoride-hydroxyl exchange in biotite. American Journal of Science, 274, 396–413.

Munoz, J.L., and Swenson, A. (1981) Chloride-hydroxyl exchange in biotite and estimation of relative HCl/HF activities in hydrothermal fluids. Economic Geology, 76, 2212–2221.

Ramberg, H. (1952) Chemical bonds and the distribution of cations in silicates. Journal of Geology, 60, 331–355.

Sisson, V.B. (1987) Halogen chemistry as an indicator of metamorphic fluid interaction with the Ponder pluton, Coast Plutonic Complex, British Columbia, Canada. Contributions to Mineralogy and Petrology, 95, 123–131.

Stormer, J.C., and Carmichael, I.S.E. (1971) Fluorine-hydroxyl exchange in apatite and biotite: A potential igneous geothermometer. Contributions to Mineralogy and Petrology, 31, 121–131.

Valley, J.W., and O'Neil, J.R. (1982) Oxygen isotope evidence for shallow emplacement of Adirondack anorthosite. Nature, 300, 497–500.

Vanko, D.A. (1986) High-chlorine amphiboles from oceanic rocks: Products of highly saline hydrothermal fluids? American Mineralogist, 71, 51–59.

Volfinger, M., Robert, J.L., Vielzeuf, D., and Neiva, A.M.R. (1985) Structural control of the chlorine content of OH-bearing silicates (micas and amphiboles). Geochimica et Cosmochimica Acta, 49, 37–48.

Yardley, B.W.D. (1985) Apatite composition and the fugacities of HF and HCl in metamorphic fluids. Mineralogical Magazine, 49, 77–79.

Manuscript received April 4, 1991
Manuscript accepted July 11, 1991